EFDA–JET–CP(14)02/03

B.A. Lomanowski, A.G. Meigs, N.J. Conway, K.-D. Zastrow, R.M. Sharples,
P. Heesterman, D. Kinna and JET EFDA contributors

Enhanced Visible and Near-Infrared Capabilities of the JET Mirror-Linked Divertor Spectroscopy System

Enhanced Visible and Near-Infrared Capabilities of the JET Mirror-Linked Divertor Spectroscopy System

B.A. Lomanowski[1], A.G. Meigs[2], N.J. Conway[2], K.-D. Zastrow[2], R.M. Sharples[1], P. Heesterman[2], D. Kinna[2] and JET EFDA contributors*

JET-EFDA, Culham Science Centre, OX14 3DB, Abingdon, UK

[1]Centre for Advanced Instrumentation, Department of Physics, Durham University, Durham, DH1 3LE, UK
[2]EURATOM-CCFE Fusion Association, Culham Science Centre, OX14 3DB, Abingdon, OXON, UK
** See annex of F. Romanelli et al, "Overview of JET Results",*
(24th IAEA Fusion Energy Conference, San Diego, USA (2012)).

Preprint of Paper to be submitted for publication in Proceedings of the
20th Topical Conference on High-Temperature Plasma Diagnostics, Atlanta, Georgia, USA
1st June 2014 – 5th June 2014

ABSTRACT

The mirror-linked divertor spectroscopy diagnostic on JET has been upgraded with a new visible and nearinfrared grating and filtered spectroscopy system. New capabilities include extended near-infrared coverage up to 1875nm, capturing the hydrogen Paschen series, as well as a 2kHz frame rate filtered imaging camera system for fast measurements of impurity (Be II) and deuterium Dα, Dβ, Dγ line emission in the outer divertor. The expanded system provides unique capabilities for studying spatially resolved divertor plasma dynamics at near-ELM resolved timescales as well as a test bed for feasibility assessment of near-infrared spectroscopy.

1. INTRODUCTION

The mirror-linked divertor spectroscopy system [1] on JET provides spatially resolved passive spectroscopy measurements of plasma emission from the outer divertor. The system covers a total spectral range of 350–1000nm. In preparation for the JET ITER-like wall (ILW) campaigns the system was upgraded in 2008 with an extended FOV (150mm to 360mm) and increased optical throughput [2].

Following the 2013 JET-ILW campaign further opportunities were identified for improving the system, namely:

- Extending the near-infrared spectral coverage to 1875nm
- Increasing the time resolution of Balmer series and Be line intensity spatially resolved measurements up to ~500μs
- Increasing the wavelength window for dedicated Balmer series measurements

Spectroscopy in the near-infrared range offers the potential of increased tolerance to the degradation of optics under a harsh burning plasma environment [3], but plasma emission in the 1000–1875nm range is poorly characterized at present.

Improved time resolution and a dedicated Balmer series monitor offer enhanced capabilities for divertor characterization and physics studies of plasma detachment. The high density, low temperature recombining region characteristic of the detached plasma regime results in a reduction of steady-state heat and particle fluxes to the divertor tiles. In ELMy H-mode plasmas this mechanism is periodically interrupted by edge localized modes (ELMs) which deposit a significant portion of the stored plasma energy onto the divertor tiles on timescales of ~100μs. The plasma dynamics and the interplay between ELM power deposition and plasma detachment are not well understood.

2. DIAGNOSTIC OVERVIEW

The new visible system consists of an additional imaging spectrometer (KT3E) and two imaging filter-scope cameras (KT3-E8TA/B) for spatially resolved Balmer series and impurity line emission measurements in the 350–700nm range. A notable feature of the grating spectrograph is the Schmidt-Czerny-Turner design which improves imaging quality over a traditional Czerny-Turner by greatly reducing astigmatism and coma across the focal plane while providing an f/4.6 input beam for increased throughput.

The near-infrared system extends the diagnostic spectral range to 1875nm. A single chord, low resolution compact spectrometer, utilizing a volume phase grating, provides surveying capability from 900-1700nm, and a filter-scope photodiode system provides access to the deuterium Paschen alpha line at 1874.6nm. Table 1 summarizes the specifications of the new visible and near-infrared systems.

3. DESIGN

A. OPTICS

The mirror-linked optical train can be conceptually visualized by unfolding the optical path and removing the flat relay mirrors. Fig.1(a) shows the remaining optical components: an objective lens (lens A), a field mirror (mirror D), and focusing optics in the roof lab. The FOV with $h_o = 360$mm is limited by the vessel port geometry (Fig.1(b)) whereas the biological penetration limits the light collection area upstream. In the roof lab, a pseudo-collimated on-axis beam of diameter $\varphi_r = 130$mm intercepts the primary mirrors of Newtonian telescopes which focus the intermediate divertor image onto the entrance slits of spectrometers KT3A, KT3B and KT3C. Off-axis points are vignetted as a function of the field angle θo by the penetration tube down to $\varphi_r \approx 90$mm.

The basis of the new optical system is the utilization of the beam area that is obstructed by the Newtonian secondary mirrors. A turning mirror placed in front of the secondary mirror thus gives access to both the visible and near-infrared arms of the beamsplitter configuration, as shown in Fig.1(c).

The turning mirror of diameter $\varphi_r = 27$mm placed behind the Newtonian secondary mirror cell becomes the aperture stop, reducing the throughput by a factor of 10 on axis and up to 22 for the maximum field angle.

B. DETECTORS

Selection of CCDs for the visible system was largely based on the application requirements for sensitivity and speed. For the new grating spectrometer (KT3E) a 1024×1024 pixel frame transfer cooled CCD (ProEM 1024B) offers excellent quantum efficiency (QE) with a peak of ~95% at 650 nm and very low dark current of 0.002 e-/pixel/s at –50°C. Frame rates are limited by the vertical shift rate in the frame transfer readout cycle.

Two interline CCD cameras (AVT Pike F-032) provide frame rates up to ~2kHz for the visible filtered imaging system (KT3-E8TA/B). Although the QE suffers due to lower fill factors, microlenses recover much of the QE with a peak of ~54% at 500nm for the KAI-0340 640×480 sensors. With fast charge transfer, short exposure times and minimized image smear, interline CCDs offer a good compromise between sensitivity and speed.

Detection in the near-infrared system (KT3D) is based on the Indium Gallium Arsenide (InGaAs) photodiode technology. Band gap energies of InGaAs detectors can be tuned by changing the composition ratio of In and Ga. The standard type offers good spectral response in the 900-1700nm range while extended-InGaAs photodiodes provide cut-offs up to 2600nm.

The near-infrared spectroscopy detectors consist of a cooled (–5°C) standard-InGaAs 256 pixel

linear array used in the grating spectrometer, and two extended-InGaAs 1 mm diameter cooled (–20°C) photodiodes for the Paschen alpha filter-scope. The two photodiodes are operated in photovoltaic mode in which the thermal or Johnson noise dominates over dark current noise [4].

C. FILTERS

The visible and near-infrared filter-scopes employ 2-cavity Fabry-Perot interference filters with a narrowband transmission profile of ~3.5×FWHM at 1% peak transmission. Filters in the visible system limit the bandpass to 1.5nm FWHM while the Paschen alpha line (Pα, 1874.6nm) and Pα background correction (1886nm) filters provide a 4.5 nm FHWM bandpass. A narrower bandpass in the near-infrared can technically be achieved but at substantial additional cost relative to the visible range filters. The small (<0.5°) incidence and field angles of the pseudo-collimated light incident on the bandpass filters result in a negligible center wavelength shift (<0.03nm) for all rays across the pupil.

4. DIAGNOSTIC PERFORMANCE

A. VISIBLE SYSTEM

The available light at the secondary turning mirrors of the new visible and near-infrared systems is estimated from

$$P_\lambda = L_\lambda \, G \, T_\lambda \tag{1}$$

where P_λ is the total photon flux [ph s^{-1} nm^{-1}] incident on the secondary turning mirror, Lλ is the averaged spectral radiance [ph s^{-1} m^{-2} sr^{-1} nm^{-1}] across the divertor FOV, G is the averaged etendue [m2 sr] across the field and T_λ is the total spectral optical transmission. Estimated values are G = $1.0^7 \times 10^{-8}$ [m2 sr] and $T_\lambda = 0.15$ in the range 300–2000nm.

Based on observations of the outer divertor deuterium ion fluxes in JET-ILW discharges [5,6] and using inverse photon efficiency (S/XB) coefficients from ADAS7 with an influx in the range $10^{21} \leq \Gamma \leq 10^{23}$ [m^{-2} s^{-1}], the expected Dα radiance averaged across the outer divertor is shown in Fig.2.(a) assuming a line of sight integration of emissivity ε through 100mm of an isothermal divertor plasma. With a 50μm slit width, 3mm image height and 200l/mm grating, the estimated signal-to-noise (SNR) for Dα spectroscopy on KT3E is $150 \leq SNR \leq 5500$ assuming a total CCD noise of 6 e^- RMS and 25fps frame rate. Similarly, the SNR for the Pike cameras with a Dα filter and a 2.4mm image height yields values of $10 \leq SNR \leq 350$ assuming 1kHz fps and 16 e^- RMS camera noise. On-chip and post-process binning will improve the SNR by a factor 3–5 for lower intensity lines.

Figure 2(a) also shows the estimated Bremsstrahlung (using the approach in Ref.8), and thermal contributions from the outer divertor plasma and tungsten tiles. Free-bound emission is ignored. Thermal emission includes a temperature dependent tungsten emissivity estimate [9]. The broadband emission was then multiplied by a 1.5nm FWHM bandpass centered on the Dα wavelength.

B. NEAR-INFRARED SYSTEM

The estimated range of hydrogen Paschen alpha (Pα, n = 4–3) radiance is shown in Fig.2(b). The

Dα/Pα ratio is in the range 10-20 for ionizing plasma conditions in the range $1 \leq T_e \leq 50$eV and $10^{19} \leq n_e \leq 10^{21}$ m^{-3}. The Paschen beta line (Pβ, n = 5–3, 1281.8nm) is weaker than Pα by a factor of 6–7 in the same range.

The NIR spectrometer and Pα filter-scope collect light from the entire divertor FOV. With a 50μm slit width, 50μm×500μm pixels, and a line width of 2.2 pixels FWHM, the estimated SNR for Pβ grating spectroscopy is $30 \leq SNR \leq 300$ at 100ms exposure.

The Pα photocurrent is estimated to be in the range $0.2 \leq i \leq 20$ YA, for which the SNR is $30 \leq SNR \leq 300$ given a detectivity $D^* = 2\times10^{12}$ [$cmHz^{1/2}/W$] at a measurement bandwidth of 20Hz. An avalanche photodiode (APD) could provide additional gain to improve the measurement bandwidth, but, although readily available in the standard-InGaAs range, an extended-InGaAs APD is currently a custom product and incurs significant additional cost.

Near-infrared measurements are complicated by a larger contribution of surface thermal emission. Fig.2(b) includes estimates of the thermal emission for representative tungsten tile temperatures with a bandpass of 4.5nm FWHM. The Bremsstrahlung contribution is also shown. Similar to the visible range, signal contamination from Bremsstrahlung only becomes significant for high electron density and low electron temperatures.

Removing the background contribution from the Pα signal is achieved by a separate 4.5nm FWHM bandpass filter offset from the Pα deuterium line by 11nm, limiting crosstalk between the two measurements to ~1%. The thermal emission adds a nonlinear component to the corrected Pα signal

$$I_{\alpha,corr}(T, L_\alpha) = I_{\alpha,Th}(T, L_\alpha) - \zeta I_{Th}(T) \quad (2)$$

where $I_{\alpha,corr}$, $I_{\alpha,Th}$, and I_{Th} are the corrected Pα intensity, combined Pα and thermal intensity, and the stand-alone thermal intensity, respectively, as a function of the tungsten tile temperature T and the FOV averaged Pα radiance L_α. Figure 3 shows the thermal background corrected calculated normalized Pα intensity as a function of tile temperature for the range of expected Pα radiance. The value of the correction factor ζ can modify the correction significantly at low Pα intensity and, in practice; the uncertainty (up to +/– 5% in Fig. 3) in the Pα measurement will become larger with increasing tile temperature.

5. INITIAL RESULTS

Preliminary results from the NIR spectrometer are shown in Fig.4 with the strong lines from intrinsic impurities (Be I, Be II, C I) and the Pβ and Pγ lines identified. Thermal emission from the stack of tungsten divertor tiles contributes a significant broadband component in the spectrum of Pulse No: 85829. A region of poor transmission around 1380nm is also evident in the raw data. The presence of the thermal spectrum reduces the dynamic range for line emission intensity measurements, but provides spectrally resolved temperature data useful for IR thermography. Quantitative measurements of spectral line emission intensities and line profiles are possible given a suitable background subtraction technique, provided the sum of emission components does not saturate the detector.

Initial results of the filtered imaging camera measurements with a Dα filter and 1kHz frame rate are shown in Fig.5 for two JET pulses exhibiting H-mode. In JET-ILW the occurrence of ELMs is indicated by the Be II line emission (527nm) as shown in Figure 5(a) and Figure 5(b) for the inner and outer divertor photo-multiplier (PMT) channels. The collapse in pedestal temperature and subsequent peak in radiated power are also consistent with ELM cycles. Dα divertor line emission is not a reliable ELM indicator when a cold and dense plasma region forms near the strike points.

The upper states of the deuterium series transitions can then be populated mainly by recombination rather than excitation, leading to a sudden dip in the Dα signal as the cold and dense region collapses during the ELM in contrast to the more common Dα spike associated with increased wall recycling. The inner and outer Dα PMT channels for Pulse No: 86421 show such an inversion, whereas the more conventional Dα spike is observed in Pulse No: 86255.

Figure 5(c) and Figure 5(d) demonstrate the first of its kind Dα measurements at ELM-resolved timescales and 1.2 mm spatial resolution along the outer divertor corresponding to the time window for the two pulses shown in Figure 5(a) and Figure 5(b). A spatial chord from the filtered camera data at R = 2.86 m is also shown in Figure 5(a) and Figure 5(b). The radial profiles exhibit the two types of Dα ELM signatures (dips vs. spikes) discussed and demonstrate the diagnostic potential for improved divertor characterization and physics studies associated with transient atomic processes in detached plasmas (e.g., profiles of the Dγ/Dα ratio using the pair of filtered imaging cameras).

ACKNOWLEDGEMENTS

This work, supported by the European Communities under the contract of Association between EURATOM and CCFE, was carried out within the framework of the European Fusion Development Agreement. The views and opinions expressed herein do not necessarily reflect those of the European Commission. The work was also partly funded by the United Kingdom Engineering and Physical Research Council under grant EP/K504178/1.

REFERENCES

[1]. A. Meigs et al., Review of Scientific Instruments **81**, 10E532 (2010).
[2]. A. Meigs et al., Proceedings of the 20th International Conference on Plasma Surface Interactions, 2012, Aachen, Germany.
[3]. V. A. Soukhanovskii., Review of Scientific Instruments **79**, 10F539 (2008).
[4]. A. Rogalski, Infrared Detectors, 2nd ed. (Taylor & Francis, Boca Raton, 2011).
[5]. F. Romanelli, Nuclear Fusion b, 104002 (2013).
[6]. A. Huber et al., Journal of Nuclear Materials **438**, S139-S147 (2013).
[7]. H. P. Summers, The ADAS User Manual, version 2.6, http://adas.phys.strath.ac.uk, 2004.
[8]. A. T. Ramsey and S. L. Turner, Review of Scientific Instruments **58**, 1211 (1987).
[9]. J.W. Davis and P.D. Smith, Journal of Nuclear Materials **233-237**(2) 1593-1596 (1996).

	Desc.	Specifications
KT3D	NIR spec., filtered P_α photo-diodes	Model (spec.): BaySpec NIRS-900-1700 Range (spec.): 900-1700 nm λ res. (spec.): 7 nm FWHM Aperture ratio: f/2.0 Time res.: 50-250 ms Spatial res.: single chord, full FOV Model (ph.diodes): Hamamatsu G12182-210K Pα filter: 4.5 nm FWHM
KT3E	0.32 m Schmidt Czerny-Turner imaging spec.	Model: Princeton Inst. IsoPlane SCT-320 Range: 350-700 nm Gratings: 200, 1200, 1800 l/mm Focal length, aperture: 0.32 m, f/4.6 Time res.: 15-40 ms Spatial res. (binned): 15 mm
KT3 E8TA/ E8TB	Filtered imaging spec.	Model: AVT Pike F-032 Filters: Dα, Dβ, Dγ, Be II 436.0/467.3 nm @ 1.5 nm FWHM Time res.: ≥500 μs Spatial res. (no binning): 1.2 mm/pixel

Table 1: System specifications

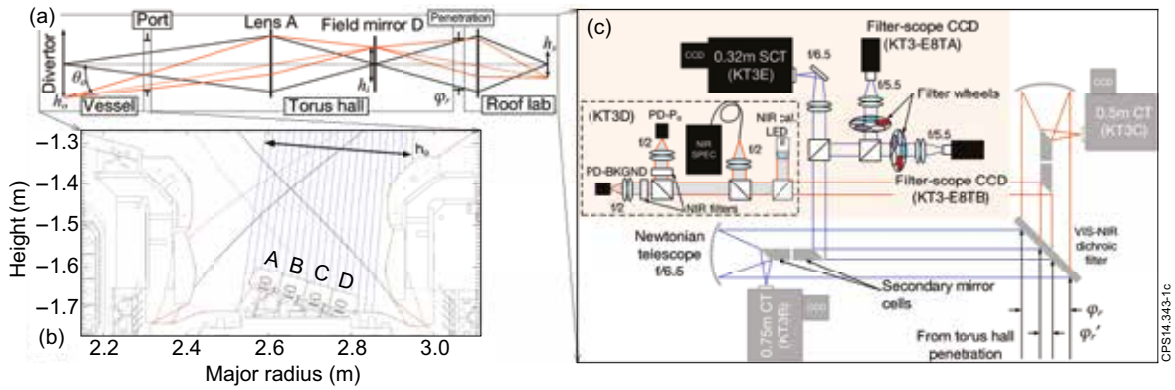

Figure 1: a) Optical layout of the mirror-linked divertor spectroscopy system; b) viewing geometry (blue) of the JETILW divertor with horizontal (magenta) and vertical (black) plasma configuration and solid horizontal tungsten tile segments A,B,C and D; c) roof lab layout of the existing (grey) and new (black) systems.

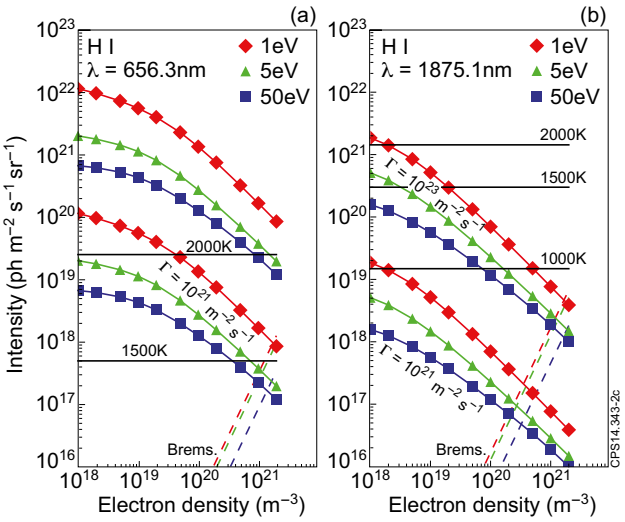

Figure 2: Line intensity estimates: a) Hα, 1.5nm FHWM bandpass; (b) Pα, 4.5nm FHWM bandpass.

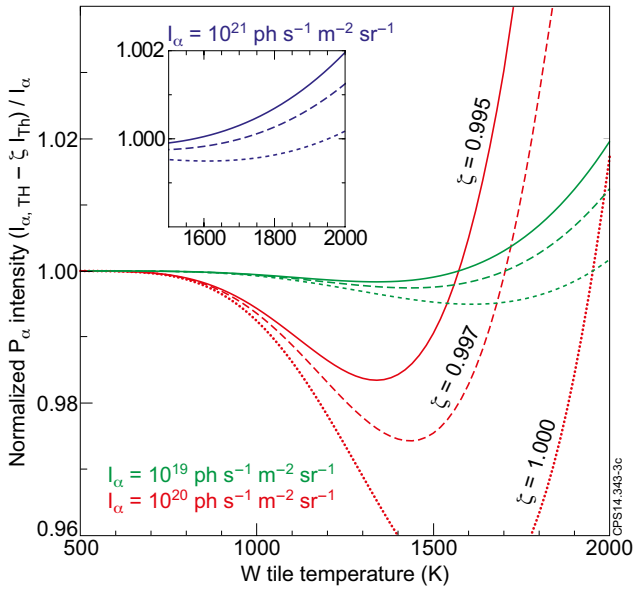

Figure 3: Calculated corrected Pα intensity for a range of given Pα intensity values.

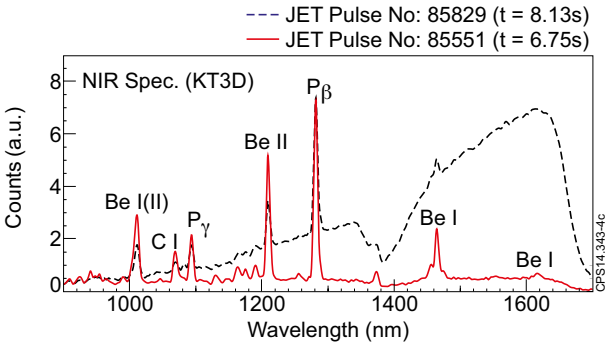

Figure 4: NIR spectra in 2.0MA, 13MW NBI and 3.3MW ICHR heated plasma (Pulse No: 85829) and 2.0MA ohmically heated plasma during a density limit disruption (Pulse No: 85551).

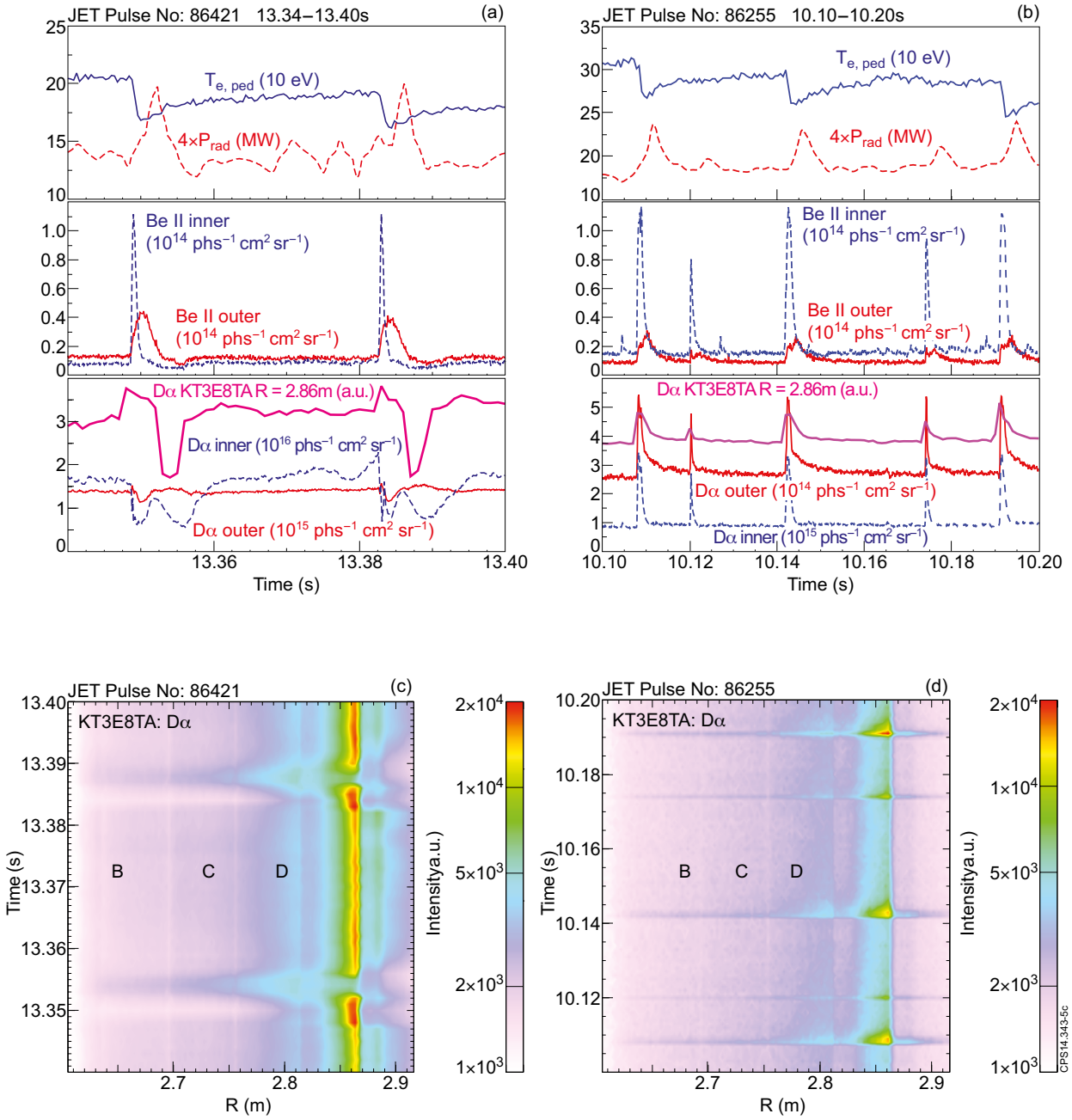

Figure 5: a) ELM cycles in JET Pulse No: 86421, 1.8MA, 2.3T, 6MW NBI; b) ELM cycles in JET Pulse No, 2.0MA, 2.9T, 7 MW NBI; c,d) Dα outer divertor radial profiles from filtered imaging camera KT3E8TA with indicated locations of the horizontal tungsten tile stacks B,C and D (see Fig.1(b) for poloidal cross section of the JET-ILW divertor).